

Asymptotics of Bayesian Error Probability and 2D Pair Superresolution

S. Prasad

Department of Physics and Astronomy, University of New Mexico, Albuquerque, New Mexico 87131

sprasad@unm.edu

Abstract: This paper employs a recently developed asymptotic Bayesian multi-hypothesis testing (MHT) error analysis [1] to treat the problem of superresolution imaging of a pair of closely spaced, equally bright point sources. The analysis exploits the notion of the minimum probability of error (MPE) in discriminating between two competing equi-probable hypotheses, a single point source of a certain brightness at the origin vs. a pair of point sources, each of half the brightness of the single source and located symmetrically about the origin, as the distance between the source pair is changed. For a Gaussian point-spread function (PSF), the analysis makes predictions on the scaling of the minimum source strength, expressed in units of photon number, required to disambiguate the pair as a function of their separation, in both the signal-dominated and background-dominated regimes. Certain logarithmic corrections to the quartic scaling of the minimum source strength with respect to the degree of superresolution characterize the signal-dominated regime, while the scaling is purely quadratic in the background-dominated regime. For the Gaussian PSF, general results for arbitrary strengths of the signal, background, and sensor noise levels are also presented.

© 2021 Optical Society of America

OCIS codes: 100.6640, 110.2960, 110.4280, 180.2520

References and links

1. S. Prasad, "Asymptotics of Bayesian error probability and rotating-PSF-based source super-localization in three dimensions;" submitted to Opt. Express.
2. For a review, see B. Huang, M. Bates, and X. Zhuang, "Super resolution fluorescence microscopy," Annual Rev. Biochem. **78**, 993-1016 (2009).
3. G. Patterson, M. Davidson, S. Manley, and J. Lippincott-Schwartz, "Superresolution imaging using single-molecule localization," Annual Rev. Phys. Chem. **61**, 345-367 (2010).
4. T. Klein, S. Proppert, and M. Sauer, "Eight years of single-molecule localization microscopy," Histochem. Cell Biol., Feb 2014 (e-print).
5. A. Gahlmann and W. Moerner, "Exploring bacterial cell biology with single-molecule tracking and super-resolution imaging," Nature Rev. Microbiol. **12**, 9-22 (2014).
6. J. Harris, "Resolving power and decision theory," J. Opt. Soc. Am. **54**, 606-611 (1964).
7. C. Helstrom, "Detection and resolution of incoherent objects by a background-limited optical system, J. Opt. Soc. Am. **59**, 164-175 (1969).
8. A. van den Bos, "Resolution in model-based measurement," IEEE Trans. Instrum. Meas. **51**, 1055-1060 (2002).
9. M. Shihram and P. Milanfar, "Imaging below the diffraction limit: a statistical analysis," IEEE Trans. Image Process. **13**, 677-689 (2004).
10. J. Chao, S. Ram, E. Sally Ward, and R. Ober, "A comparative study of high resolution microscopy imaging modalities using a three-dimensional resolution measure," Opt. Express **17**, 24377-24402 (2009).
11. S. Ram, E. Sally Ward, and R. Ober, "How accurately can a single molecule be localized in three dimensions using a fluorescence microscope?," Proc. SPIE **5699**, pp. 426-435 (2005).

12. C. Rushforth and R. Harris, "Restoration, resolution, and noise, J. Opt. Soc. Am. **58**, 539-545 (1968).
13. M. Bertero and C. De Mol, "Superresolution by data inversion, Progress in Optics **XXXVI**, 129-178 (1996).
14. E. Kosarev, "Shannon's superresolution limit for signal recovery," Inverse Prob. **6**, 55-76 (1990).
15. E. Boukouvala and A. Lettington, "Restoration of astronomical images by an iterative superresolving algorithm, Astron. Astrophys. **399**, 807-811 (2003).
16. C. Matson and D. Tyler, "Primary and secondary superresolution by data inversion, Opt. Express **14**, 456-473 (2006).
17. S. Prasad and X. Luo, "Support-assisted optical superresolution of low-resolution image sequences: the one-dimensional problem Opt. Express **17**, 23213-23233 (2009).
18. R. Gerchberg, "Superresolution through error energy reduction, Opt. Acta **21**, 709-721 (1974).
19. D. Fried, "Analysis of the CLEAN algorithm and implications for superresolution, J. Opt. Soc. Am. A **12**, 853-860 (1995).
20. P. Magain, F. Courbin, and S. Sohy, "Deconvolution with correct sampling, Astrophys. J. **494**, 472-477 (1998).
21. J. Starck, E. Pantin, and F. Murtagh, "Deconvolution in astronomy: a review," Publ. Astron. Soc. Pacific **114**, 1051-1069 (2002).
22. R. Puetter and R. Hier, "Pixon sub-diffraction space imaging, Proc. SPIE **7094**, 709405 (2008).
23. L. Lucy, "Statistical limits to superresolution," Astron. Astrophys. **261**, pp. 706-710 (1992).
24. R. Thompson, D. Larson, and W. Webb, "Precise nanometer localization analysis for individual fluorescent probes, Biophys. J. **82**, 2775-2783 (2002).
25. J. Enderlein, E. Toprak, and P. Selvin, "Polarization effect on position accuracy of fluorophore localization," Opt. Express **14**, 8111-8120 (2006).
26. S. Ram, E. Sally Ward, and R. Ober, "Beyond Rayleigh's criterion: a resolution measure with application to single-molecule microscopy," Proc. Natl. Acad. Sci. USA **103**, 4457-4462 (2006).
27. C. Leang and D. Johnson, "On the asymptotics of M-hypothesis Bayesian detection, IEEE Trans. Inf. Theory **43**, 280282 (1997). Image Process. **13**, 677689 (2004).
28. S. Prasad, "New error bounds for M-testing and estimation of source location with subdiffractive error," J. Opt. Soc. Am. A **29**, 354-366 (2012).
29. S. Smith, "Statistical resolution limits and the complexified Cramér-Rao bounds," IEEE Trans. Signal Process. **53**, 1597-1609 (2005).
30. G. Carrier, M. Krook, and C. Pearson, *Functions of a Complex Variable*, McGraw Hill (New York, 1966), Sec. 2.8,

1. Introduction

Recent ground-breaking advances in fluorescent biomarker microscopy [2] have enabled the localization and tracking of single molecules at scales of mere tens of nanometers, scales that are 10-20x finer than those achieved by the more traditional diffraction limited microscopy. As the need for rapid localization and tracking has grown, the question of disambiguation of multiple point sources in close vicinity of one another has also become important. At the most elementary level, one must characterize well the minimum SNR requirements on finely resolving a single pair of equally bright point sources with a given sub-diffractive separation under varying levels of background, sensor, and signal noise. Such a characterization is critical to the design and construction of ever more capable microscopes that must perform these tasks with exquisite spatio-temporal resolution in our effort to understand biological processes at the cellular level.

We recently analyzed [1] the minimum probability of error (MPE) in the localization of a single molecule to sub-diffractive scales. Our statistical approach employed the Bayesian multi-hypothesis testing (MHT) protocol that for the problem of transverse (2D) localization assigns *a priori* equal probability, $1/M_{\perp}^2$, that the molecule is located in any one of $M_{\perp} \times M_{\perp}$ possible equal-area square subcells into which a chosen square base-resolution cell may be subdivided. The image data, essentially the point-spread function (PSF) of the imaging system corrupted by a variety of noise sources, including background, sensor, and photon noise, add information about the source location, helping thus to reduce the MPE from $1 - 1/M_{\perp}^2$, that for the equi-probable prior alone, to a value that can be bounded below by means of the maximum *a posteriori* probability (MAP) criterion for choosing the decision regions. If the data are of a sufficiently high quality, then the MPE can dip below a certain threshold value, say 5%

corresponding to a statistical confidence limit (CL) of 95%, for localizing the molecule with M_{\perp} times higher linear precision along each transverse dimension. This 2D localization error analysis was extended to include the axial, or depth, dimension as well. A complete analysis, including its asymptotics, of the minimum signal strengths needed for super-localizing a point source to ever smaller spatial scales in both transverse and axial dimensions under varying background and sensor noise conditions was presented in Ref. [1].

The present paper specializes our MHT-based MPE analysis to the related problem of super-resolution imaging of multiple point sources that are closely separated and thus subject to being confused as a single point source of the same intensity as the combined intensity of the individual sources. This is particularly true if the spacing is well within the Abbe diffraction limit, $0.61\lambda/NA$, of a microscope operating with numerical aperture NA and imaging wavelength λ . However, as a number of recent experimental results have shown [3, 4, 5], the diffraction limit furnishes a nominal benchmark at best, and improvements well beyond it are eminently possible based on diffraction-limited far-field image data.

Here we ask and answer, in the Bayesian MPE framework, the elementary question: What source brightness is needed to reduce the MPE below a given threshold for discriminating a single pair of closely spaced, equally bright point sources of a given separation from a single point source of the same brightness located at the midpoint of the line joining the pair? This defines a simpler problem of *binary* hypothesis testing within the Bayesian detection framework, avoiding a more involved problem in which the matter of such binary *discrimination* is coupled with the additional requirement of *estimating* the spacing between the point-source pair. The minimum signal strengths needed for this single source vs. pair source discrimination, as we shall see, are rather modest and consistent with the growing experimental evidence for high-precision optical superresolution (OSR) of point sources.

Similar questions of source-pair OSR in the framework of Bayesian inference have been asked previously by others [6, 7, 8, 9]. These analyses are more limited, however, because they either employ simplifying assumptions such as one-dimensional PDFs or do not account for non-Gaussian sources of noise and consider the full range of noise sources from additive sensor noise to signal and background-based shot noise comprehensively. Considerations of the minimum requirements for superresolution of closely spaced point sources have recently gained prominence in view of highly developed experimental techniques for superresolution fluorescence microscopy [2] for localizing single biolabel fluorophors that are now quite the rage in live-cell biological and biomedical imaging.

The limits on the spatial resolution of a closely spaced pair of point sources have been examined previously [10] in the context of biomolecular microscopy by means of a non-Bayesian estimation-theoretic analysis involving the Cramér-Rao lower bound (CRB) on an unbiased estimation of their mutual spacing. This analysis, while exhaustive in terms of the orientation and the location of the midpoint of the separation vector near the in-focus plane of a conventional clear-circular-aperture imager, was largely numerical, providing only limited insights into the minimum requirements, e.g., on the combined source strength, to resolve a specific subdiffraction separation in the presence of varying amounts of background and sensor noise levels. Even more importantly, this analysis suffers from the same weakness as any other CRB-based analysis in requiring certain regularity conditions for its validity, including a non-vanishing local first-order derivative of the statistical distribution of the data with respect to (w.r.t.) the parameter being estimated. This specific condition breaks down when the sources are located along the optical axis and their separation vector is centered at the in-focus plane where the imager PSF has a vanishing first-order derivative w.r.t. the axial coordinate and the CRB in fact diverges [11] as a result.

The general OSR problem subsumes a large collection of well defined problems, a fact that

merits some discussion here. The many claims and counter-claims of the possibility of OSR debated over the past several decades have as much to do with the complexity of proper analysis as with the nature of the specific OSR problem being considered. At the risk of over-simplification, we sharpen this debate with the mention of two specific OSR problems here. For one, the prohibitively difficult prospects of bandwidth extension beyond the diffraction limited cut-off by means of data inversion performed by imposing physical constraints [14, 12, 13, 15, 16, 17] constitute a very different problem from that of superresolving point sources. The degree of bandwidth extension is typically logarithmic in the signal-to-noise ratio (SNR), a fact that is also well understood from Shannon’s channel capacity theorem [14]. But the knowledge that all sources in a scene are point-like, rather than being extended with arbitrary variations of brightness across them, is sufficiently information-bearing that superresolving them to well within the diffraction limit requires, as we hope to prove, rather more modest source-signal strengths. Independent confirmations of this claim are provided by a number of studies involving actual computational algorithms, including those presented in [18, 19, 20, 21, 22]. These algorithms make use, in essential ways, of the point-like extension of sources being reconstructed from noisy, filtered image data.

It is also worth noting that Lucy’s early analysis [23] of the point-source OSR problem in which he derived a prohibitive eighth-power scaling of the minimum source strength w.r.t. the pair separation was based on his asking a different question: What source strength is needed to disambiguate this pair from a single *extended*, spatially symmetric source of the same source strength and the same second-order spatial moment of the intensity distribution? Here the alternative (“null”) hypothesis involves an extended source of the same root-mean-squared (RMS) width as the separated source-pair in the main hypothesis. It is this additional constraint of equal RMS width placed on the two hypotheses that renders pair OSR so much harder to achieve in his analysis.

We begin this paper with a brief review of our earlier analysis [1] of the MPE as applied to the problem of super-localizing a single point source in three dimensions. The specialization of this multi-hypothesis testing (MHT) analysis and its asymptotic considerations to the present problem of pair OSR in the single transverse plane of best focus appear in Sec. 3, where we further specialize the problem to the case of a Gaussian model PSF. This restriction to the Gaussian PSF shape, rather than the Bessel-function-based Airy-disk PSF, is not essential but does enable a more transparent and complete analytical treatment. The biomolecular localization microscopy literature [24, 2] on the specific form of the in-focus PSF is divided, since the presence of any residual aberrations in the optics and the dipolar emission pattern [25] from a fluorophore typically predispose a single-molecule image to deviate significantly from the Airy form, so the more generic bell-shaped form is as good, typically, as any other to assume. Our considerations may, however, be adapted to a completely general image form by means of a Taylor expansion to the second order along the lines of References [9, 26]. For the Gaussian PSF, we derive detailed expressions for the MPE and also their asymptotic form for signal and background dominated regimes, including an important logarithmic correction to the quartic scaling law for the minimum photon strength needed for a sought pair OSR enhancement factor in the strong-signal regime. In Sec. 4, we present and discuss the results of a numerical evaluation of our analytical expressions, involving certain numerically ill-behaved logarithmic integrals derived in Sec. 3, for arbitrary relative strengths of the signal and background levels. We conclude the paper in Sec. 5 with a brief summary and outlook of the work.

2. A Brief Review of our Previous Asymptotic MHT Analysis

Let the conditional statistics of the data X be specified by a probability density function (PDF), $P(x|m)$, conditioned on the validity of a specific hypothesis \mathcal{H}_m , labeled by an integer m ,

$m = 1, \dots, M$. In the Bayesian framework, the posterior distribution, $P(m|x)$, quantifies the information carried by the data about the likelihood of the hypothesis \mathcal{H}_m having given rise to the observed data. The maximum *a posteriori* (MAP) estimator provides one fundamental metric of minimum error, namely the MPE, in correctly identifying the operative hypothesis under all possible observations,

$$P_e^{(min)} = 1 - \mathbb{E}[P(\hat{m}_{MAP} | X)], \quad (1)$$

where \hat{m} is the MAP estimator,

$$\hat{m}_{MAP}(X) = \arg \max_{m=1, \dots, M} P(m | X). \quad (2)$$

Expression (1) may be reformulated by means of the Bayes rule as a double sum of data integrals,

$$P_e^{(min)} = \sum_{m=1}^M p_m \sum_{m' \neq m} \int_{\mathcal{R}_{m'}} dx P(x | m) \quad (3)$$

over the various decision regions $\mathcal{R}_{m'}$ chosen according to the MAP protocol.

When many observations are involved, as, e.g., for the typical image dataset consisting of N pixels with $N \gg 1$, $P_e^{(min)}$ may be evaluated approximately under conditions of moderate to high SNR by replacing the inner sum over m' in Eq. (3) by a single term \tilde{m} that labels the decision region “closest” to \mathcal{R}_m in the following sense:

$$\tilde{m} = \arg \max_{m' \neq m} \max_{x \in \mathcal{R}_{m'}} \{P(x | m)\}. \quad (4)$$

The MPE is thus accurately approximated by the asymptotic expression

$$P_e^{(min)} = \sum_{m=1}^M p_m \int_{\mathcal{R}_{\tilde{m}}} dx P(x | m) \quad (5)$$

at sufficiently high values of the SNR.

For the case of image data acquired under combined signal photon-number fluctuations, background fluctuations, and sensor read-out noise, the following pseudo-Gaussian conditional data PDF accurately describes the statistics of data at least at large photon numbers:

$$P(x | m) = \frac{1}{(2\pi)^{N/2} \det^{1/2}(\Sigma_m)} \exp[-(1/2)(x^T - x_m^T) \Sigma_m^{-1} (x - x_m)]. \quad (6)$$

where, under the condition of statistically independent data pixels, the data covariance matrix is a diagonal matrix of the form¹

$$\Sigma_m = \text{diag}(\sigma^2 + b + x_m), \quad (7)$$

where σ_2 , b , and $x_m \in \mathbb{R}^N$ denote, respectively, the variance of sensor read-out noise, the mean background count, assumed spatially uniform, and the mean signal vector, given the hypothesis m .

For this problem, we derived in Ref. [1] the following expression valid in the asymptotic limit of high photon numbers, many pixels, and hypotheses that are hard to discriminate from

¹ We use here a shorthand notation, $\text{diag}(v)$, for specifying a diagonal matrix whose diagonal elements are the elements of v taken in order. Similarly, $\text{diag}(u/v)$, denotes the diagonal matrix of elements that are ratios of the corresponding elements of the vectors u and v . In Matlab, this would be the element-wise quotient, $u./v$, of the two vectors of which the diagonal matrix is formed.

one another because the corresponding mean signal vectors that separate their statistics are very similar:

$$P_e^{(min)} = \frac{1}{2} \sum_m p_m \operatorname{erfc} (\|U_m\|_2 / \sqrt{2}), \quad (8)$$

where $\|U_m\|_2$ takes the asymptotic form

$$\|U_m\|_2 = \frac{1}{2} \frac{\sum_{i=1}^N \frac{(\sigma^2 + b + x_{mi})^{1/2}}{(\sigma^2 + b + \bar{x}_{mi})^2} (\delta x_{\bar{m}mi})^2}{\left[\sum_{i=1}^N \frac{1}{(\sigma^2 + b + \bar{x}_{mi})^2} (\delta x_{\bar{m}mi})^2 \right]^{1/2}} \quad (9)$$

in terms of the components of the vector separation, $\delta x_{\bar{m}mi}$, between the mean data vectors for the nearest-neighbor decision-region pairs \mathcal{R}_m and $\mathcal{R}_{\bar{m}}$, as defined by relation (4). The arithmetic mean, \bar{x}_m , of the mean signal vectors in the two decision regions that occurs in this expression may be replaced by either mean signal vector, say x_m , as we do presently, without incurring significant error in the asymptotic limit as defined above.

3. Bayesian MPE Analysis for the Point-Source-Pair Superresolution Problem

As we have indicated earlier, the problem of discriminating a pair of closely spaced point sources from a single point source is a binary hypothesis testing (BHT) problem in which the sum (9) is limited to two terms only, $m = 1$ and $m = 2$ corresponding to the cases of a single point source and a pair of point sources, respectively. Since the passage from the double sum (3) to the single sum (5) is exact for the BHT problem, any error involved in the expression (8) is only due to any asymptotic analysis of the full MPE contribution from each decision region. In the asymptotic limit and for only two terms in the sum (8), the two norms, $\|U_1\|_2$ and $\|U_2\|_2$, as defined by relation (9) are essentially the same, namely

$$\|U_0\|_2 \stackrel{\text{def}}{=} \frac{1}{2} \frac{Q}{R^{1/2}}, \quad (10)$$

where Q and R are defined as the sums

$$\begin{aligned} Q &\stackrel{\text{def}}{=} \sum_{i=1}^N \frac{1}{(\sigma^2 + b + x_{1i})^{3/2}} (x_{2i} - x_{1i})^2; \\ R &\stackrel{\text{def}}{=} \sum_{i=1}^N \frac{1}{(\sigma^2 + b + x_{1i})^2} (x_{2i} - x_{1i})^2. \end{aligned} \quad (11)$$

Since the priors add to 1, $p_1 + p_2 = 1$, the MPE (8) thus reduces to the simple form

$$P_e^{(min)} = \frac{1}{2} \operatorname{erfc} (\|U_0\|_2 / \sqrt{2}). \quad (12)$$

For the 2D imaging problem at hand, the single sum over the elements i in each of our above expressions expands into a double sum over the pixel indices i and j .

In the following analysis we shall restrict our attention to a circular Gaussian-shaped PSF that is azimuthally invariant in the $\xi\eta$ image plane,

$$H(\xi, \eta) = \frac{1}{2\pi w^2} \exp \left[-\frac{(\xi^2 + \eta^2)}{2w^2} \right], \quad (13)$$

which is normalized to have unit volume, $\int \int d\xi d\eta H(\xi, \eta) = 1$, as appropriate for the PSF of a lossless imager. The continuous PSF (13) may be approximated by its discrete form, taking

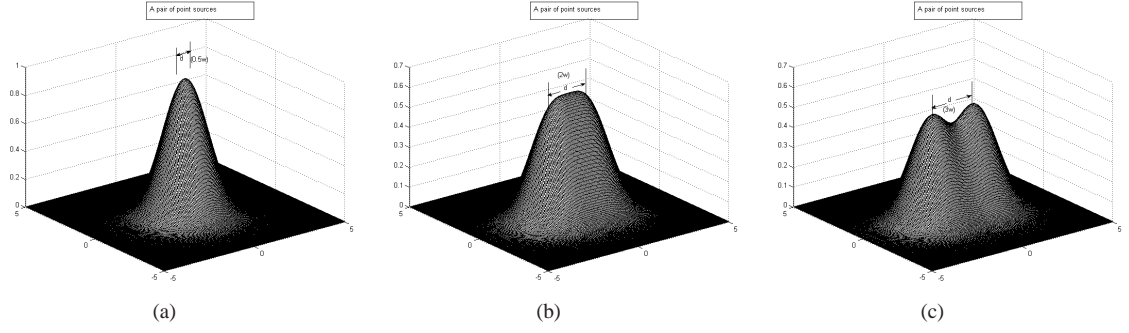


Fig. 1: The image of a pair of point sources of equal brightness under the Gaussian-shaped PSF (14), for (a) $d/w = 0.5$; (b) $d/w = 2$; and (c) $d/w = 3$.

the following value on the (i, j) th pixel, centered the point (ξ_{ij}, η_{ij}) :

$$H_{ij} = \frac{1}{2\pi w^2} \exp \left[-\frac{(\xi_{ij}^2 + \eta_{ij}^2)}{2w^2} \right] \Delta A, \quad (14)$$

in which ΔA is the area of each of the many square pixels over which the PSF is assumed to be distributed. In the discrete form (14), the PSF is normalized approximately as

$$\sum_{i,j} H_{ij} = 1, \quad (15)$$

a relation that becomes exact in the limit $\Delta A \rightarrow 0$.

The two hypotheses in the present problem are characterized by the mean signals, x_1 and x_2 , that are given in terms of the discrete PSF (14) as

$$\begin{aligned} x_{1ij} &= K H_{1ij} = \frac{K}{2\pi w^2} \exp \left[-\frac{\xi_{ij}^2 + \eta_{ij}^2}{2w^2} \right] \Delta A; \\ x_{2ij} &= K H_{2ij} \\ &= \frac{K}{4\pi w^2} \left\{ \exp \left[-\frac{(\xi_{ij} - d/2)^2 + \eta_{ij}^2}{2w^2} \right] + \exp \left[-\frac{(\xi_{ij} + d/2)^2 + \eta_{ij}^2}{2w^2} \right] \right\} \Delta A, \end{aligned} \quad (16)$$

in which K is the source strength in units of photon number, d is the spacing between the point sources, assumed to be situated on the ξ axis, and the two data mean vectors have expanded to become matrices supported on the pixel array for the 2D imaging problem. The quantum efficiency (QE) is assumed to be 1 here, but an imperfect QE is easily included by multiplying both K and b by it in all of the expressions. Figure 1 shows examples of the image (16) for the point-source pair for three different values of the ratio d/w .

With the elements of the data-mean matrices given by Eqs. (16), let us now expand each term in the numerator Q of the MPE expression, defined by relation (11), in a power series in K , interchange the order of the resulting infinite sum and the pixel sum, and then perform the pixel sum by means of its continuous version. We arrive in this way at the following expression

for Q :

$$Q = \frac{K^2 \Delta A}{(2\pi w^2)(\sigma^2 + b)^{3/2}} \sum_{n=0}^{\infty} \frac{(-1)^n (2n+1)!!}{n!(n+2)} \left[\frac{K \Delta A}{2(\sigma^2 + b)2\pi w^2} \right]^n \times \left[1 + \frac{1}{2} e^{-\frac{nd^2}{4(n+2)w^2}} - 2e^{-\frac{(n+1)d^2}{8(n+2)w^2}} + \frac{1}{2} e^{-\frac{d^2}{4w^2}} \right], \quad (17)$$

in which the double factorial is defined as $(2n+1)!! = 1.3 \dots (2n+1)$, namely the product of all odd integers from 1 to $(2n+1)$. The evaluation of simple Gaussian integrals needed to arrive at this result is presented in Appendix A. Expression (17) may be further simplified in the limiting case of interest, namely when $d \ll w$, by expanding the exponentials inside the square brackets in powers of d/w . The lowest-order term that survives in such an expansion is quartic and, following straightforward algebra, shown to have the value,

$$\left(\frac{d^2}{8w^2} \right)^2 \frac{(n^2 + 2n + 3)}{(n+2)^2},$$

so to this order the following expression for Q results:

$$Q = \frac{K^2 \Delta A (d/w)^4}{(128\pi w^2)(\sigma^2 + b)^{3/2}} \sum_{n=0}^{\infty} \frac{(-1)^n (2n+1)!!}{n!(n+2)} \times \frac{(n^2 + 2n + 3)}{(n+2)^2} \left[\frac{K \Delta A}{2(\sigma^2 + b)2\pi w^2} \right]^n. \quad (18)$$

By means of the identity,

$$\frac{n^2 + 2n + 3}{(n+2)^2} = 1 - \frac{2}{n+2} + \frac{3}{(n+2)^2},$$

we may express Q as

$$Q = \frac{K^2 \Delta A (d/w)^4}{(128\pi w^2)(\sigma^2 + b)^{3/2}} [q_1(u) - 2q_2(u) + 3q_3(u)], \quad (19)$$

where the three q 's and u are defined by the relation

$$q_k(u) \stackrel{\text{def}}{=} \sum_{n=0}^{\infty} \frac{(-1)^n (2n+1)!!}{2^n n! (n+2)^k} u^n, \quad u \stackrel{\text{def}}{=} \frac{K \Delta A}{2\pi w^2 (\sigma^2 + b)}. \quad (20)$$

The quantity q_k may be evaluated recursively for increasing values of k by a simple mathematical trick. Note first that $u^2 q_k(u)$ is simply the integral, from 0 to u , of the sum

$$\sum_{n=0}^{\infty} \frac{(-1)^n (2n+1)!!}{2^n n! (n+2)^{k-1}} v^{n+1},$$

which is simply v times $q_{k-1}(v)$,

$$u^2 q_k(u) = \int_0^u v q_{k-1}(v) du. \quad (21)$$

Since $q_0(u)$ is simply the power-series expansion of $(1+u)^{-3/2}$, valid for $|u| < 1$, we may evaluate the q_k successively for increasing integer values of k as

$$\begin{aligned} u^2 q_1(u) &= \int_0^u dv \frac{v}{(1+v)^{3/2}} \\ &= \int_0^u dv \left[\frac{1}{(1+v)^{1/2}} - \frac{1}{(1+v)^{3/2}} \right] \\ &= 2(1+u)^{1/2} + 2(1+u)^{-1/2} - 4; \end{aligned} \quad (22)$$

$$\begin{aligned} u^2 q_2(u) &= 2 \int_0^u dv v^{-1} [(1+v)^{1/2} + (1+v)^{-1/2} - 2] \\ &= 4 \left(\sqrt{1+u} - 1 \right) - 8 \ln \left(\frac{1 + \sqrt{1+u}}{2} \right); \end{aligned} \quad (23)$$

and

$$u^2 q_3(u) = 4 \int_0^u \frac{dv}{v} \left[(1+v)^{1/2} - 1 \right] - 8 \int_0^u \frac{dv}{v} \ln \left(\frac{1 + \sqrt{1+v}}{2} \right). \quad (24)$$

The details of the evaluation of integral (23) are presented in Appendix B, while integral (24), obtained by a substitution of expression (23) into relation (24) for $k = 3$, must be evaluated numerically.

These expressions for the various q 's when computed and substituted into expression (19) evaluate Q fully. Note that while the power series expansions on which expression (19) is based are valid only when $|u| < 1$, the expressions (22)-(24) are valid for arbitrary values of u except where they fail to be analytic. This is guaranteed by the principle of analytic continuation [30].

Expression (11) for R , which determines the denominator of the MPE expression (10), may be evaluated quite similarly as Q . In the small-spacing limit, $d/w \ll 1$, one may again substitute $K H_{1ij}$ for x_{1ij} and $K H_{2ij}$ for x_{2ij} , in that sum expression for R , then expand each term in the resulting expression in powers of K , interchange the power series sum with the pixel sum, and evaluate the latter, which in view of expressions (16) for H_{1ij} and H_{2ij} involves only Gaussian functions, approximately by converting it into an integral over the full $\xi \eta$ plane. Term by term, the Gaussian integrals are the same ones we evaluated for Q , so their lowest-order limiting form in powers of d/w is again quartic, and the following expression for R results:

$$\begin{aligned} R &= \frac{K^2 \Delta A (d/w)^4}{(128 \pi w^2) (\sigma^2 + b)^2} \sum_{n=0}^{\infty} \frac{(-1)^n (n+1)}{(n+2)} \\ &\quad \times \frac{(n^2 + 2n + 3)}{(n+2)^2} \left[\frac{K \Delta A}{2 \pi w^2 (\sigma^2 + b)} \right]^n. \end{aligned} \quad (25)$$

By means of the identity,

$$\frac{n^2 + 2n + 3}{(n+2)^2} = 1 - \frac{2}{n+2} + \frac{3}{(n+2)^2},$$

we may express R as

$$R = \frac{K^2 \Delta A (d/w)^4}{(128 \pi w^2) (\sigma^2 + b)^2} [r_1(u) - 2r_2(u) + 3r_3(u)], \quad (26)$$

where u is defined in Eq. (20) and the three r 's are defined as the power series

$$r_k(u) \stackrel{\text{def}}{=} \sum_{n=0}^{\infty} \frac{(-1)^n (n+1)}{(n+2)^k} u^n, \quad k = 1, 2, 3. \quad (27)$$

Like the q 's, the r 's too may be evaluated recursively by means of an analogous integral relation they obey, namely

$$u^2 r_k(u) = \int_0^u v r_{k-1}(v) dv. \quad (28)$$

Since $r_0(u)$ given by (27) for $k = 0$ is simply the Taylor expansion of $(1 + u)^{-2}$, we have

$$\begin{aligned} r_1(u) &= \frac{1}{u^2} \int_0^u \frac{v}{(1+v)^2} dv \\ &= \frac{1}{u^2} \int_0^u \left[\frac{1}{1+v} - \frac{1}{(1+v)^2} \right] dv \\ &= \frac{1}{u^2} \left[\ln(1+u) + \frac{1}{1+u} - 1 \right] = \frac{1}{u^2} \ln(1+u) - \frac{1}{u(1+u)}. \end{aligned} \quad (29)$$

From this expression for $r_1(u)$, we may now express $r_2(u)$ as the integral

$$\begin{aligned} r_2(u) &= \frac{1}{u^2} \int_0^u dv \left[\frac{\ln(1+v)}{v} - \frac{1}{(1+v)} \right] \\ &= \frac{1}{u^2} \left[\int_0^u dv \frac{\ln(1+v)}{v} - \ln(1+u) \right], \end{aligned} \quad (30)$$

and, recursively, $r_3(u)$ as

$$\begin{aligned} r_3(u) &= \frac{1}{u^2} \int_0^u \frac{dv}{v} \left[\int_0^v dw \frac{\ln(1+w)}{w} - \ln(1+v) \right] \\ &= \frac{1}{u^2} \int_0^u (\ln u - \ln v) \frac{\ln(1+v)}{v} - \frac{1}{u^2} \int_0^u \frac{dv}{v} \ln(1+v), \end{aligned} \quad (31)$$

where to reach the second equality we needed to perform an integration by parts of the double integral in the first equality. These integral forms for r_2 and r_3 may be evaluated numerically, and R given by Eq. (26) thus fully calculated, with validity guaranteed for arbitrary values of the argument u by analytic continuation.

In terms of the quantities q_k and r_k we have just calculated, we may now express the argument of the erfc function in the MPE expression (10) via relations (19) and (26) as

$$\frac{\|U_0\|_2}{\sqrt{2}} = \frac{K\Delta A^{1/2}(d/w)^2}{16[(4\pi w^2)(\sigma^2 + b)]^{1/2}} \frac{[q_1(u) - 2q_2(u) + 3q_3(u)]}{[r_1(u) - 2r_2(u) + 3r_3(u)]^{1/2}}, \quad (32)$$

in which u , defined by Eq. (20) as the ratio of the characteristic number of mean signal photons per pixel, $K\Delta A/(2\pi w^2)$, and the sum of the background and sensor noise variances per pixel, $\sigma^2 + b$, is a measure of the SNR for the problem. We take $b \gg \sigma^2$ in all our numerical evaluations, in which case u may be interpreted as the signal-to-background ratio (SBR). We now develop limiting analytical forms for the right-hand side (RHS) of this expression in the photon-signal-dominated and background-dominated regimes, given by $u \gg 1$ and $u \ll 1$, respectively.

3.1. Photon-Signal-Dominated Regime, $u \gg 1$

In this regime, we may use asymptotic forms of the various p 's and q 's occurring in expression (32). The following asymptotic forms, as we show in Appendix C, are obtained in the limit

$u \rightarrow \infty$:

$$\begin{aligned} q_1(u) &\sim \frac{2}{u^{3/2}}; \quad q_2(u) \sim \frac{4}{u^{3/2}}; \quad q_3(u) \sim \frac{8}{u^{3/2}}; \\ r_1(u) &\sim \frac{\ln u}{u^2}; \quad r_2(u) \sim \frac{1}{2u^2}[(\ln u)^2 - 2\ln u]; \quad r_3(u) \sim \frac{1}{u^2} \left[\frac{(\ln u)^3}{6} - \frac{(\ln u)^2}{2} \right]. \end{aligned} \quad (33)$$

With these asymptotic forms and definition (20) for u , expression (32) may be approximated as

$$\begin{aligned} \frac{\|U_0\|_2}{\sqrt{2}} &= \frac{K\Delta A^{1/2}(d/w)^2}{16[(4\pi w^2)(\sigma^2 + b)]^{1/2}} \frac{18\sqrt{2}}{\sqrt{u} \ln^{3/2}(u)} \\ &= \frac{9\sqrt{K}d^2/w^2}{8\ln^{3/2}(u)}. \end{aligned} \quad (34)$$

Let us set the threshold on the MPE at p as the minimum requirement on the fidelity of Bayesian discrimination between the single-point-source and symmetric binary-source hypotheses. A typical value taken for p is 0.05, corresponding to a statistical CL of 95%, but one can adjust p according to the stringency of the application. Equating the RHS of relation (12) to p and solving for the argument of the erfc function in terms of the inverse function, which we may denote erfc^{-1} , we require that $\|U_0\|_2/\sqrt{2}$ have the minimum value

$$\frac{\min \|U_0\|_2}{\sqrt{2}} = \text{erfc}^{-1}(2p) \quad (35)$$

and thus, from the asymptotically valid relation (34), arrive at the following implicit value of the minimum photon number, K_{min} , needed to achieve this fidelity:

$$K_{min} = \left[\frac{8\text{erfc}^{-1}(2p)}{9} \right]^2 \frac{w^4}{d^4} \ln^3 \left[\frac{K_{min}\Delta A/(2\pi w^2)}{(b + \sigma^2)} \right]. \quad (36)$$

Expression (36) exhibits a nearly quartic scaling of the minimum photon number needed to discriminate a point-source pair from its single-point-source equivalent, as a function of the inverse spacing d^{-1} between the source pair. Specifically, this scaling is given by the ratio $(w/d)^4$, namely the fourth power of the ratio of the characteristic width of the PSF and the spacing between the source pair being resolved, that is modified by a logarithmic dependence on the SNR. The latter factor increases relatively slowly with increasing K_{min} , but tends to exacerbate somewhat a purely quartic scaling of K_{min} as higher and higher values of the pair-OSR factor, w/d , are sought. Such logarithmic factors have not been predicted by previous researchers [7, 23, 9, 29], as their analyses have not been sufficiently comprehensive in treating the full range of combined noise statistics. Further, the analyses of Ref. [7, 9] assumed essentially white Gaussian additive noise, rather than photon-number-dominated Poisson noise treated here, and their power SNR scales quadratically, rather than linearly, with the photon number. This difference of the noise statistics accounts for their quadratic, rather than our essentially quartic, scaling of K_{min} on the degree of pair OSR sought.

In spite of its modification by a logarithmic correction, the quartic scaling of K_{min} is considerably more modest than the eighth-power scaling predicted by Lucy [23] for a similar problem. As we have argued earlier, the assumption of a single point source in our analysis, rather than a single equivalent but extended source in Lucy's analysis, for the "null" hypothesis of an unresolved source potentially provides more constraining information that an algorithm can make essential use of to resolve the source pair at a more modest signal strength.

3.2. Background-Noise-Dominated Regime, $u \ll 1$

In the limit $u \rightarrow 0$, the various q and r functions tend to the same values, $q_k = r_k = (1/2)^k$, so the ratio involving them in expression (32) simplifies to $(3/8)^{1/2}$

$$\frac{\|U_0\|_2}{\sqrt{2}} = \sqrt{\frac{3}{8}} \frac{K\Delta A^{1/2}(d/w)^2}{16[(4\pi w^2)(\sigma^2 + b)]^{1/2}}, \quad (37)$$

so the minimum photon number needed for a pair superresolution factor of amount w/d is now expected to scale only quadratically with that factor, without any logarithmic corrections. For a fidelity denoted by the MPE threshold p , we may perform a similar analysis as for the photon-signal-dominated regime of the previous sub-section to arrive at the following expression for K_{min} :

$$\frac{K_{min}\Delta A^{1/2}(d/w)^2}{16[(4\pi w^2)(\sigma^2 + b)]^{1/2}} = \sqrt{\frac{8}{3}} \operatorname{erfc}^{-1}(2p). \quad (38)$$

4. Numerical Results and Discussion

In Figs. 2(a)-(c), we plot the RHS of the exact result (32) as a function of the photon number K for three different background variance levels, b , and illustrate the transition from the quadratic scaling of the background-dominated regime to the approximately quartic scaling of the signal-dominated regime of operation of our Gaussian-PSF-based imager. In each plot, the sensor noise variance σ^2 has been set equal to 1, while the ratio of the characteristic area under the PSF to the pixel area, $2\pi w^2/\Delta A$, is set to 100. For the case of a low background level, $b = 10^2$, even at the lowest source strength plotted in Fig. 2(a), namely $K = 10^2$, the signal-to-background photon ratio (SBR) u , defined by relation (20), is at its lowest value comparable to 1. At much higher source strengths of interest, $K > 10^4$, $u \gg 1$ and the plot displays the decrease of the MPE with increasing signal strength appropriate to the signal-dominated regime in which the approximation (34) for the argument of the erfc function is quite accurate. The different curves in the plots refer to different values of the OSR ratio w/d , starting at 2 (denoted as 1x) and increasing to 20 (denoted as 10x), with the higher w/d values requiring higher source strengths to bring the error down to the CL threshold. The bottom figure, Fig. 2(c), displays the MPE behavior in the opposite limit of background-dominated operation in which at the largest source strength, $K = 10^{11}$, the ratio u is 1, and for all others it is less than 1, being in fact considerably smaller than 1 over the range of source strengths over which the MPE decreases from its highest value of 0.5 toward the statistical-confidence-level (CL) threshold of 0.05. The upper right figure, Fig. 2(b), displays the results for the case for which its left half represents the background-dominated regime of operation and the right half the signal-dominated regime. Note an appreciable but expected rightward shift in the MPE curves as the spatially uniform background level increases from one figure to the next. As the background level increases, it becomes increasingly harder, requiring increasingly higher source strengths, to discriminate between the null and alternative hypotheses.

The variation of the minimum photon number required to achieve the CL threshold as a function of the OSR ratio, w/d , is plotted in Fig. 3 for the three different background levels of Fig. 2. The values of this number were simply read off from the intersections of the MPE curves in Figs. 2 with the CL threshold line. The doubly logarithmic plots show the expected nearly quartic and quadratic scaling with w/d for the photon-dominated and background-dominated regimes, while for the intermediate background level, $b = 10^6$, the scaling is nearly quadratic for the smaller d/w values for which K_{min} is smaller than or comparable to $(2\pi w^2/\Delta A)$, or 100, times b , but for larger w/d , the slow change of slope consistent with the nearly quartic scaling of the signal-dominated regime can be discerned. The transition from slope-2 to slope-4 is rather gradual, taking several decades of increase in K_{min} to complete.

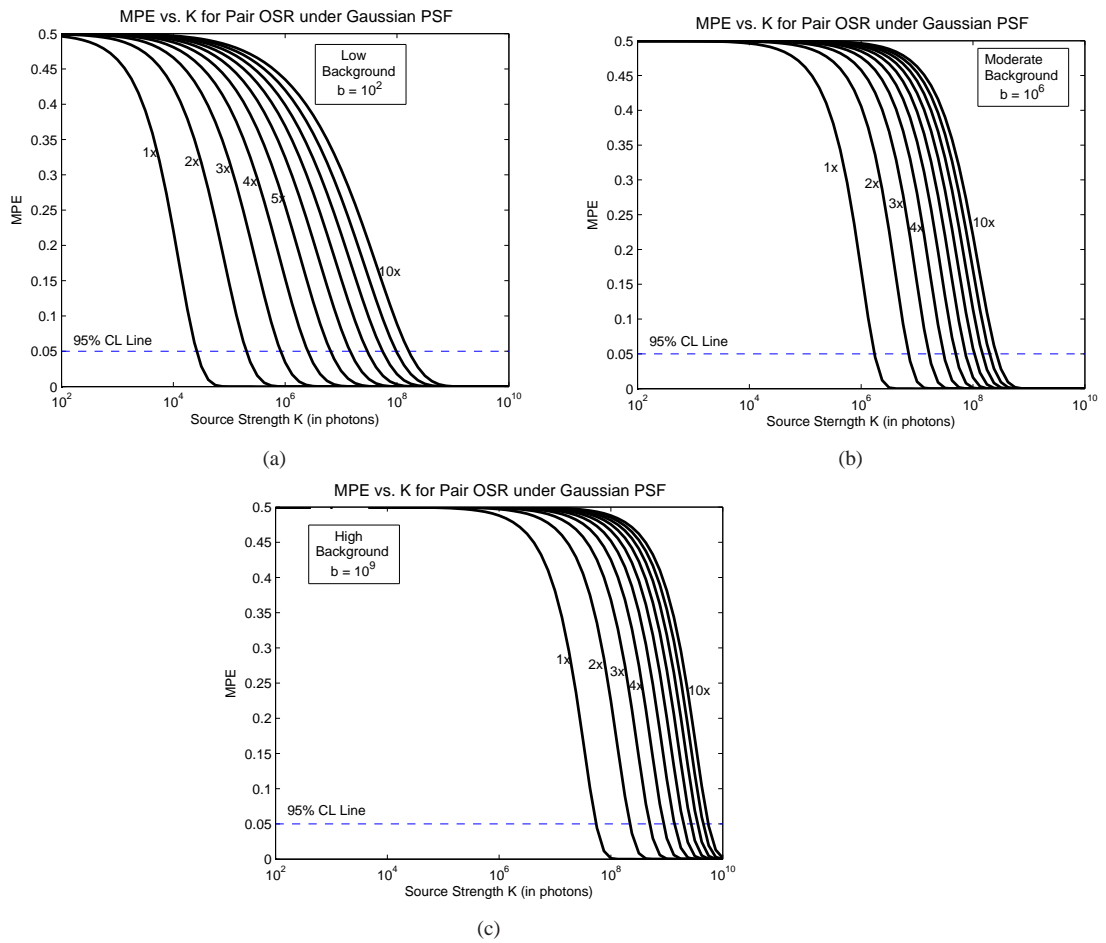


Fig. 2: A plot of MPE vs. signal strength for three different background levels. (a) $b = 10^2$; (b) $b = 10^6$; and (c) $b = 10^9$.

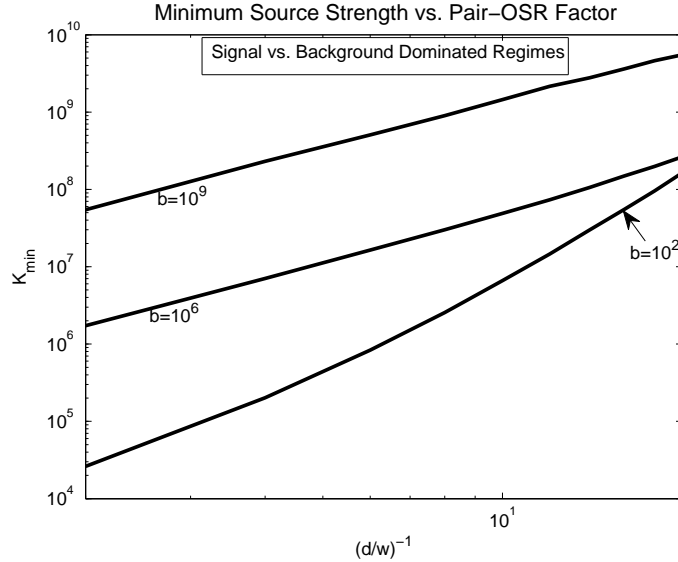


Fig. 3: Log-log plots of the minimum source strength, K_{min} , vs. the OSR ratio, w/d , for the same three different background levels as in Figs. 2.

It is rather remarkable that one can achieve *any* OSR at all when the spatially uniform mean background level and its shot-noise fluctuations dominate, as in Fig. 2(c), the signal part of the data with its information-bearing spatial variations that are consistent with the background-free image of a separated source pair. The higher source strengths needed when even relatively small OSR ratios are sought, as seen in Fig. 3, confirm the difficulty of attaining OSR in the background-dominated regime. The change of slope of the $\ln w/d$ vs. $\ln K_{min}$ curve from 4 to 2 as the background gets stronger relative to the signal must mean that the various curves in Fig. 3 must asymptote to the same limit as the degree of sought OSR and the corresponding K_{min} are increased to still greater values not shown in the plot.

It is worth noting that the sensor and background variances per pixel occur together in all our expressions as $\sigma^2 + b$. In the pseudo-Gaussian approximation for the PDF for combined sensor, background, and signal photon-number fluctuations, the various noise sources are equivalent. However, that is not so in a more accurate treatment needed to incorporate either background or signal photon-number fluctuations at much lower strengths of order 10 or lower, where their discrete Poisson statistics can no longer be approximated well by a continuous Gaussian PDF.

5. Conclusions

In this paper we have presented a detailed Bayesian error analysis based on binary-hypothesis testing (BHT) to derive expressions for the minimum combined source strength needed to superresolve a pair of closely spaced point sources located in the plane of best focus from their image formed under a Gaussian PSF approximation. The statistical metric we have used here to determine this minimum value of the source strength needed for pair OSR is the minimum probability of error (MPE) on a successful BHT protocol. Specifically, we considered the pair to be resolved if the MPE for the associated BHT problem falls below a small threshold value, taken here to be 0.05. Our calculations are done for a variety of operating conditions characterized by arbitrary values of the source signal strength, background photon count, and sensor noise variance.

Our detailed quantitative calculations predict an approximately quartic dependence of the minimum source strength on the reciprocal of the pair spacing in the regime where the signal dominates the background. This scaling of source strength with respect to the inverse spacing is in fact slightly steeper than quartic via a multiplicative correction that is logarithmic in the ratio of the signal and background levels. In the opposite limit of the background-dominated regime of operation, this scaling is more modestly quadratic.

The problem of pair OSR when the sources are along the optical axis and thus in a common line of sight (LOS) is expected to entail much steeper scaling of minimum source power with inverse spacing in both the signal-dominated and background-dominated regimes. The main reason for this difference of on-axis, or longitudinal, OSR from the transverse OSR treated in the present paper is that in the former case, unlike the latter, the PSF has no first order sensitivity on the spacing, which must imply more stringent requirements on any LOS pair OSR. However, the mathematical divergences seen in local first-order analyses using the Cramér-Rao lower bound on unbiased estimation are expected to be moderated in a Bayesian analysis that includes in effect non-vanishing higher-order sensitivities of the data PDF on the parameter being estimated, here the pair spacing. This problem will be treated in a subsequent paper.

Acknowledgments

Helpful conversations with Rakesh Kumar, Srikanth Narravula, Julian Antolin, Henry Pang, and Keith Lidke are gratefully acknowledged. The work reported here was supported in part by AFOSR under grant numbers FA9550-09-1-0495 and FA9550-11-1-0194.

A. Certain Gaussian Integrals

The following integral over the full $\xi\eta$ plane must be evaluated to arrive at expression (17):

$$\int d\xi d\eta \exp\left[-\frac{n(\xi^2 + \eta^2)}{2w^2}\right] \left\{ \exp\left[-\frac{\xi^2 + \eta^2}{2w^2}\right] - \frac{1}{2} \exp\left[-\frac{(\xi - d/2)^2 + \eta^2}{2w^2}\right] - \frac{1}{2} \exp\left[-\frac{(\xi + d/2)^2 + \eta^2}{2w^2}\right] \right\}^2. \quad (39)$$

Squaring the terms inside the braces and then multiplying out the Gaussian functions in the integrand yields four different kinds of Gaussian integrals, each over the $\xi\eta$ plane, namely

$$\begin{aligned} I_0 &\stackrel{\text{def}}{=} \int \exp\left[-\frac{(\xi^2 + \eta^2)(n+2)}{2w^2}\right] d\xi d\eta; \\ I_{\pm} &\stackrel{\text{def}}{=} \int \exp\left[-\frac{(n+1)\xi^2 + (\xi \mp d/2)^2 + (n+2)\eta^2}{2w^2}\right] d\xi d\eta; \\ J_{\pm} &\stackrel{\text{def}}{=} \int \exp\left[-\frac{n\xi^2 + 2(\xi \mp d/2)^2 + (n+2)\eta^2}{2w^2}\right] d\xi d\eta; \text{ and} \\ J_0 &\stackrel{\text{def}}{=} \int \exp\left[-\frac{n\xi^2 + (\xi - d/2)^2 + (\xi + d/2)^2 + (n+2)\eta^2}{2w^2}\right] d\xi d\eta. \end{aligned} \quad (40)$$

The first of these integrals is simply evaluated as

$$I_0 = \frac{2\pi w^2}{n+2}. \quad (41)$$

The remaining integrals are evaluated by “completing the square” in each Gaussian exponent

that contains unshifted and shifted quadratic expressions. Thus, for example,

$$(n+1)\xi^2 + (\xi \mp d/2)^2 = (n+2) \left[\xi \mp \frac{d}{2(n+2)} \right]^2 + \frac{(n+1)d^2}{4(n+2)}, \quad (42)$$

a trick that, when used in the exponent of the second of the Gaussian integrals, I_{\pm} , in relation (40), followed by an appropriate finite shift of the infinite range of the integral, enables us to evaluate the ξ part of the integral. The η part of the double integral in each of these integral expressions is always the same, and evaluates to $\sqrt{2\pi w^2/(n+2)}$. Accounting for the left-over terms like $(n+1)d^2/[4(n+2)]$ in each exponent of the ξ -dependent integrand then yields the following evaluations for the remaining integrals:

$$\begin{aligned} I_{\pm} &= \frac{2\pi w^2}{(n+2)} \exp \left[-\frac{d^2}{8w^2} \left(\frac{n+1}{n+2} \right) \right]; \\ J_{\pm} &= \frac{2\pi w^2}{(n+2)} \exp \left[-\frac{d^2}{4w^2} \left(\frac{n}{n+2} \right) \right]; \text{ and} \\ J_0 &= \frac{2\pi w^2}{(n+2)} \exp \left[-\frac{d^2}{4w^2} \right]. \end{aligned} \quad (43)$$

B. Evaluation of Integral (23)

By writing, $v = \sinh^2 \alpha$, and noting that $1 + v = \cosh^2 \alpha$, we may simplify integral (23) as

$$\begin{aligned} & 2 \int_0^{\sinh^{-1} \sqrt{u}} d\alpha \frac{(\cosh \alpha - 1)^2}{\sinh \alpha} \\ &= 4 \int_0^{\sinh^{-1} \sqrt{u}} d\alpha \frac{\sinh^3(\alpha/2)}{\cosh(\alpha/2)}, \end{aligned} \quad (44)$$

where we obtain the second line from the first by means of the identities, $\cosh \alpha = 1 + 2\sinh^2(\alpha/2)$ and $\sinh \alpha = 2\sinh(\alpha/2)\cosh(\alpha/2)$. We now make another substitution, $\beta = \cosh(\alpha/2)$, and note that $d\beta = \sinh(\alpha/2)d\alpha/2$ to reduce the above integral expression to the form,

$$8 \int_1^{\cosh(\sinh^{-1} \sqrt{u}/2)} d\beta \frac{\beta^2 - 1}{\beta}. \quad (45)$$

This integral is easily evaluated as

$$\begin{aligned} & 4 [\cosh^2(\sinh^{-1} \sqrt{u}/2) - 1] - 8 \ln \cosh(\sinh^{-1} \sqrt{u}/2) \\ &= 4 \sinh^2(\sinh^{-1} \sqrt{u}/2) - 4 \ln \left[\frac{1 + \cosh(\sinh^{-1} \sqrt{u})}{2} \right] \\ &= 2 [\cosh(\sinh^{-1} \sqrt{u}) - 1] - 4 \ln \left(\frac{1 + \sqrt{1+u}}{2} \right) \\ &= 2 [\sqrt{1+u} - 1] - 4 \ln \left(\frac{1 + \sqrt{1+u}}{2} \right), \end{aligned} \quad (46)$$

where we used simple hyperbolic-function identities, $\cosh^2 \alpha = 1 + \sinh^2 \alpha$ and $1 + 2\sinh^2(\alpha/2) = 2\cosh^2(\alpha/2) - 1 = \cosh \alpha$, to reduce the various expressions to their final form.

C. Asymptotic Forms of the Various q and r Functions

From expressions (22) and (23), the large- u approximations for $q_1(u)$ and $q_2(u)$ follow quite simply, since for $u \gg 1$ any positive power of u dominates any constants or logarithms of u or negative powers of u ,

$$q_1(u \gg 1) \sim \frac{2}{u^{3/2}}, \quad q_2(u \gg 1) \sim \frac{4}{u^{3/2}}. \quad (47)$$

For large u , the integrals in Eq. (24) representing $u^2 q_3(u)$ may be approximated by approximating their integrands near the upper limit u ,

$$\frac{[(1+v)^{1/2} - 1]}{v} \sim v^{-1/2}, \quad \ln\left(\frac{1 + \sqrt{1+v}}{2}\right) \sim \frac{1}{2} \ln v, \quad (48)$$

so the two integrals may be evaluated straightforwardly near the upper limit and the following expression for $q_3(u)$, valid for $u \gg 1$, results:

$$q_3(u \gg 1) \sim \frac{8}{u^{3/2}} - \frac{2}{u^2} \ln^2(u) \sim \frac{8}{u^{3/2}}, \quad (49)$$

where we have ignored, in the second approximate equality, the second term of the first approximate equality as being logarithmically smaller for sufficiently large u for which $u^{-1/2} \ln^2 u \ll 4$.

Similar considerations give us the asymptotic forms for $r_k(u)$, $k = 1, 2, 3$. From the last equality in Eq. (29), it follows that $r_1(u \gg 1) \sim u^{-2} \ln u$. We may now determine the approximate form for $r_2(u)$ for $u \gg 1$ by approximating the integrand of the integral in expression (30) as $v^{-1} \ln v$, whose integral is easily evaluated near the upper limit as $(1/2) \ln^2 u$. The following asymptotically valid form for $r_2(u)$ is thus obtained:

$$r_2(u \gg 1) \sim \frac{1}{2u^2} (\ln^2 u - 2 \ln u). \quad (50)$$

Finally, a similar approximation, $\ln(1+v) \approx \ln v$, in the integrand of expression (31) for $r_3(u)$ enables us to evaluate the integral near its upper limit u , for $u \gg 1$, as

$$\begin{aligned} r_3(u) &\sim \frac{1}{u^2} \left(\frac{\ln^3 u}{2} - \frac{\ln^3 u}{3} - \frac{\ln^2 u}{2} \right) \\ &= \frac{1}{u^2} \left(\frac{\ln^3 u}{6} - \frac{\ln^2 u}{2} \right). \end{aligned} \quad (51)$$

In deriving expressions (50) and (51), we have been careful to retain terms that are logarithmic in u as being comparable to numerical constants of order 1.